The International Journal of Advanced Manufacturing Technology (2018) 99:951–963
https://doi.org/10.1007/s00170-018-2456-1

ORIGINAL ARTICLE

Research on the axial stiffness softening and hardening characteristics of machine tool spindle system

Jiandong Li[1] · Yongsheng Zhu[1] · Ke Yan[1] · Xiaoyun Yan[1] · Yuwei Liu[1] · Jun Hong[1]

Received: 28 February 2018 / Accepted: 17 July 2018 / Published online: 15 August 2018

Abstract

Bearing stiffness exhibits non-linear characteristic when the bearing is subjected to a certain external load, which will inevitably cause changes in the spindle stiffness, since bearing stiffness has a decisive impact on the spindle stiffness. In this paper, the axial stiffness softening and hardening characteristics of machine tool spindle were studied. A novel spindle axial load automatic applying device and the spindle stiffness test bench were proposed. Meantime, an axial stiffness model for the experimental spindle was established based on the bearing load–displacement model and mechanical analysis of spindle. Then, the axial stiffness of fixed position preload spindle under different preload was measured experimentally and the evolution mechanism was analyzed. The results show that when bearing preload reaches a certain relatively large threshold, a "sag" shape occurs in the axial stiffness curve, indicating the "stiffness hardening" characteristic of the spindle. On the other hand, for a small preload, no "sag" shape occurs in spindle stiffness curve, indicating the "stiffness softening" characteristic of the spindle. This phenomenon is of great significance for the acquisition of the excellent spindle stiffness properties.

Keywords Machine tool · Spindle system · Stiffness hardening · Stiffness softening · Bearing preload · Axial stiffness

Nomenclature

A_o	Distance between groove curvature centers
d_b	Ball diameter.
d_m	Bearing pitch diameter
E	Young's modulus of material
E^*	Equivalent Young's modulus
F_{ab}	Axial load applied to bearing
k_{a1}	Axial stiffness of front bearing
k_{a2}	Axial stiffness of rear bearing
k_a	Axial stiffness of spindle
K_f	Load-deflection coefficient of bearing
k_i	Load-deflection coefficient of inner ring
k_o	Load-deflection coefficient of outer ring
R	Groove curvature radius
Z	Number of balls

Greek letters

α	Operating contact angle of bearing
α_f	Initial contact angle of bearing
δ_1	Pre-deflection of front bearing
δ_2	Pre-deflection of rear bearing
δ_1'	Deflection of front bearing
δ_2'	Deflection of rear bearing
δ_a	Displacement of spindle
δ_{ab}	Axial deflection of bearing
δ_p	Initial deflection of bearing
δ_z	Critical deflection of bearing
ν	Poisson's ratio of the material
ρ_1	Principal curvature in lateral direction
ρ_2	Principal curvature in rolling direction

Subscripts

b	ball
i	inner ring
ir	inner ring material
o	outer ring
or	outer ring material

✉ Yongsheng Zhu
yszhu@mail.xjtu.edu.cn

[1] Key Laboratory of Education Ministry for Modern Design and Rotor-Bearing System, Xi'an Jiaotong University, Xi'an 710049, China

1 Introduction

Spindle-bearing system is the core component of high precision machine tools, which greatly affects the accuracy of the whole manufacturing process [1]. Spindle stiffness, as one of the most important indicators for evaluating spindle performance, directly influents the processing quality of the machine tool during the machining process [2]. For drilling machine, vertical spindle surface grinder and machining centers for boring and drilling operations, the axial stiffness of spindle–bearing system becomes the primary factor affecting spindle performance because the axial load is the main cutting force of the spindle during its operation [3]. The design of spindle stiffness faces several critical issues. One of them is on the acquisition of the excellent stiffness properties. Generally, preload is provided for the spindle–bearing system to adjust spindle stiffness [4]. However, the preload will change with the operating condition of a spindle–bearing system [5–7]. It, therefore, creates the need to gain the required spindle stiffness by quantitatively applying the preload.

Bearing is the major component of the spindle, and its stiffness has a decisive impact on the spindle stiffness [8]. Tlusty et al. [9] found that the stiffness of preloaded bearing has the characteristics of "softening" spring. Similarly, Chen et al. [8] found that the bearing stiffness presents a non-linear effect during the operating condition. Soon and Stone [10] studied the nonlinear characteristics of the bearing stiffness. Different operating conditions will cause softening and hardening effects of the bearing stiffness. Lin et al. [6] predicted that the bearing preload influences the bearing stiffness. The above research on bearing stiffness provides the basis for the study of spindle stiffness. Moreover, the non-linear characteristic of the bearing stiffness will inevitably cause changes in the spindle stiffness, since the bearing stiffness determines the overall spindle-bearing stiffness [11, 12].

In the stiffness research on machine tool spindle, Matsubara et al. [1] proposed a non-contact measurement method of spindle radial stiffness by using magnetic loading device. Similarly, Sarhan et al. [13, 14] investigated the effects of temperature and speed on the spindle radial stiffness by using displacement sensors. The study of radial stiffness provides a reference for the measurement of the spindle axial stiffness. In addition to speed and temperature, the external load can also affect the spindle stiffness due to the nonlinear property of the bearing stiffness. Tsuneyoshi [15] proposed a contact type loading device for the measurement of spindle axial load. The axial load–displacement curve obtained by that loading device exhibits a nonlinear relationship. The work provided a basic approach for the further analysis of the relationship between external load and spindle axial stiffness. Li et al. [16] proposed a mathematical model for spindle axial stiffness analysis. However, only constant pressure preload was discussed. As fixed position preload method and constant pressure preload method are totally different, the axial stiffness evolution mechanism of fixed position preload spindle is much different with that of constant pressure preload spindle [17]. It is a pity that, in all the above researches, the stiffness softening and hardening characteristics of the machine tool spindle caused by nonlinear bearing stiffness have not been revealed.

In this paper, a novel testing method was proposed to experimentally study the spindle stiffness softening and hardening properties. For experimental purpose, a new spindle axial load automatic applying device and axial displacement measurement approach were proposed, and a special test bench was designed to measure the spindle stiffness under different preload. In order to explain the experimental results, the axial stiffness model of the experimental spindle was established by considering the non-linearity of spindle bearing stiffness, and the evolution mechanism of spindle axial stiffness was theoretically analyzed.

2 Experimental study on spindle axial stiffness

At present, there are mainly two methods for measuring the spindle stiffness: force deflection method and natural frequency method [18]. The former calculates the spindle stiffness by measuring the acting force and the corresponding displacement of spindle, while the latter first gets the natural frequency of the spindle, and then obtains the spindle stiffness by inquiring the predefined frequency–stiffness relationship. Generally, natural frequency method is greatly affected by many factors such as the installation of the spindle or the connection stiffness of the spindle and the base, so its test accuracy is limited [15], and force deflection method is widely used in the field of spindle stiffness testing.

2.1 Design of the stiffness testing equipment

Force deflection method involves two key technologies: load applying technology and displacement measurement technology. Currently, loading unit of the stiffness testing equipment includes magnetic, pneumatic, and hydraulic types [1, 19]. The magnetic type can easily cause electromagnetic interference to the displacement sensors of the spindle test system, thereby reducing test accuracy [20]. The loading stability is poor for pneumatic type loading unit due to the relatively large compressibility of gas. Compared with the other two types, the hydraulic loading unit has strong loading capacity and stability, but its accessory system is more complex and inconvenient to use [21]. In order to measurement displacement accurately, high precision eddy current, inductive, or capacitive displacement sensors are normally used [22]. Due to the limitation of the frequency response of the inductive

displacement sensor and the susceptibility to dust and oil of capacitive displacement sensor, eddy current displacement sensor is the first choice for displacement measurement of spindle in stiffness testing experiments [23].

In this paper, a novel spindle axial stiffness test device was designed, in which a mechanical load applying unit and three eddy sensors were adopted, as shown in Figs. 1 and 2. Figure 1 gives the basic structure of the load applying unit, which is mainly composed of a tool holder, loading components, a ball guide sleeves, a force knob, a motor, etc. The tool holder is used to connect the experimental spindle and the motor drives the force knob to rotate so as to apply the axial load to the spindle through the loading components. The ball guide sleeves are adopted to constrain the loading components to move axially within the cylindrical sleeve so as to eliminate the interference of the eccentric load. In addition, the loading components involve the disc springs, pull-pressure sensor, and ball bearings. The disc spring plays the buffer effect and reduces the loading increment through its own deformation. The pull-pressure sensor is used for measuring the load applied to the spindle, while the ball bearings provide the basis for the future study on the effects of speed on the spindle stiffness. Figure 2 shows the displacement measurement scheme of the spindle stiffness. The displacement of the target plate fixed to the tool holder is monitored and measured by the eddy current displacement sensor uniformly distributed in the circumferential direction since axial centerline displacement of the spindle cannot be directly measured. The measured results are averaged to be defined as the actual displacement of the spindle. Finally, the axial load and axial displacement data are automatically uploaded to the computer software via the acquisition equipment (MÜLLER-BBM®). The specific parameters of the pull-pressure sensor and displacement sensor are shown in Table 1.

2.2 Experimental test of spindle stiffness

In the aspect of the spindle stiffness data processing and analysis, the traditional test method is to acquire the load and corresponding displacement data of the spindle based on the larger thrust load increment (namely, the number of test points is less). Then, the least square method is adopted to fit the load and displacement data, and the slope of the fitted curve is supposed to be the spindle stiffness (illustrated in Fig. 3) [24]. However, the spindle stiffness is considered to be constant in this method and the nonlinearity of the bearing stiffness is ignored [25]. In fact, external load affects the load distribution and ball–raceway contact state of bearing [26], which in turn affects the bearing stiffness as well as the stiffness of the spindle [27]. It is a pity that the external load applied to the spindle is often not enough to fully reflect the variation of the spindle stiffness based on the traditional test method.

For the sake of analyzing the spindle stiffness more comprehensively and accurately, a novel spindle stiffness test method was proposed. In order to comprehensively study the evolution of spindle stiffness, it is necessary to increase the range of external load applied to the spindle, and the maximum load must exceed the unloading load of the spindle bearing. Specifically, the maximum load should not exceed 6 times than initial preload. Moreover, the maximum load cannot exceed the axial limit load of bearing to avoid damage to the bearing. Considering the possible difference in the bearing type between the two ends of the spindle, tension and thrust loads are applied to the spindle to obtain two-way stiffness in the test. At the same time, in order to increase the density of the data to observe the nonlinear property of the stiffness, relatively high sampling frequency is adopted to acquire the load and displacement data. The stiffness of

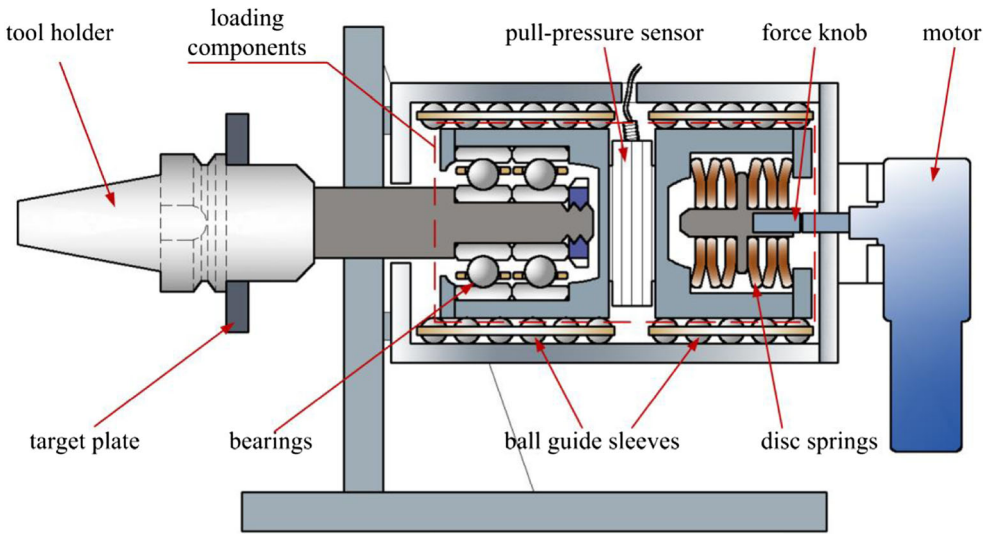

Fig. 1 The structure of the novel load applying unit

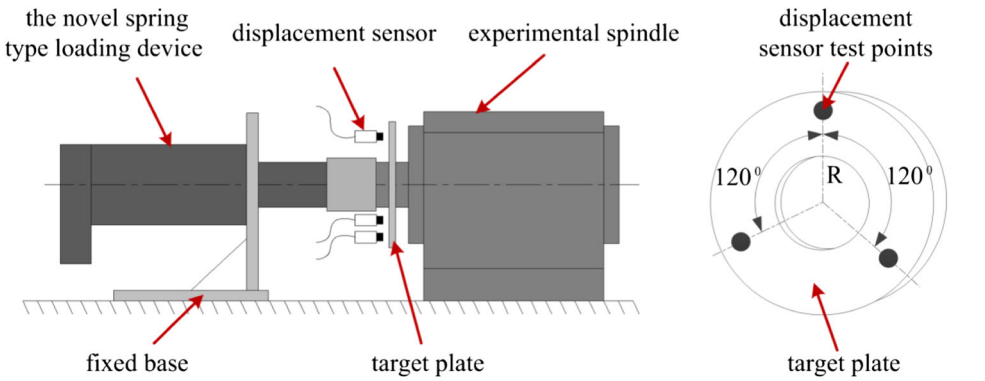

(a) spindle stiffness test rig (b) displacement sensor layout

Fig. 2 The displacement measurement scheme of the spindle stiffness

spindle is calculated from detailed load–displacement data with the derivative method, as given in Eq. (1).

$$k_a = \frac{\mathrm{d}F_a}{\mathrm{d}\delta_a} \tag{1}$$

where k_a is the spindle axial stiffness; F_a means the axial load applied to the spindle, and δ_a indicates the spindle axial displacement.

A test rig was constructed to experimentally study the spindle axial stiffness, as shown in Fig. 4. The experimental spindle is a fixed position preload mechanical spindle, and its structure is shown in Fig. 5. The spindle is supported by two angular contact ball bearings; this kind of bearing has advantages of high stiffness, high accuracy and ability to withstand axial loads, and therefore is widely used in high-speed spindle [28]. The preload of bearing can be controlled by adjusting the width difference between the inner and outer spacers. In this paper, the spindle axial stiffness at three different preload levels (see Table 2) is tested respectively to observe the influence of preload on spindle axial stiffness.

Table 1 The specific parameters of the pull-pressure sensor and displacement sensor

Sensor	Pull-pressure sensor	Displacement sensor
Type	HBM® U3-5KN	KAMAN® KF2306-5SUM
Measurement range	− 5000 N–5000 N	500 μm
Sensor resolution	0.5 N	0.1 μm
Allowable overload measurement range	50%	
Relative zero signal deviation	< 1%	
Effect of temperature on sensitivity/10 K (by reference to nominal sensitivity)	< 0.1%	The sensor is equipped with a temperature compensation module
Effect of temperature on zero signal/10 K (by reference to nominal sensitivity)	<0.1%	

2.3 Experimental results

The axial stiffness of the experimental spindle under different preload was tested, and the experimental results are shown in Fig. 6. It can be found that the overall rigidity of spindle increases as the preload increases. For example, in case of the same axial displacement, the axial stiffness of the spindle under preload 290 N is greater than 145 N, and the axial stiffness under preload 740 N is the largest. At the same time, it can be seen from Fig. 6 that the stiffness curve is asymmetric with respect to zero point of the displacement since the stiffness of draw bar mechanism is coupled into the spindle stiffness during the pulling process.

It is also found that at the mutation point of the spindle stiffness curve, the greater the preload is, the larger the axial displacement of the spindle becomes. For example, the mutation of the stiffness curve for preload of 145 N, 290 N, and 740 N occurs at about − 0.007 mm, − 0.010 mm, and − 0.019 mm separately. This means that, in the spindle design stage, the appropriate preload should be selected according to the operating load of the spindle. Otherwise, the mutation of spindle stiffness will affect the machining quality of the workpiece.

Furthermore, before the spindle stiffness mutation occurs, there is a very obvious "sag" phenomenon in the stiffness curve of the spindle with a preload of 740 N, which is known as the "stiffness hardening" characteristics of the spindle (the spindle stiffness increases with the increase of axial load after ignoring the tilted trend caused by draw bar mechanism's stiffness). In contrast, this phenomenon does not appear for the situation of preload of 145 N and 290 N. For the case of preload 145 N, the stiffness decreases with the increase of the axial load in both pulling and pushing process. That is, the spindle has the characteristics of "stiffness softening". While

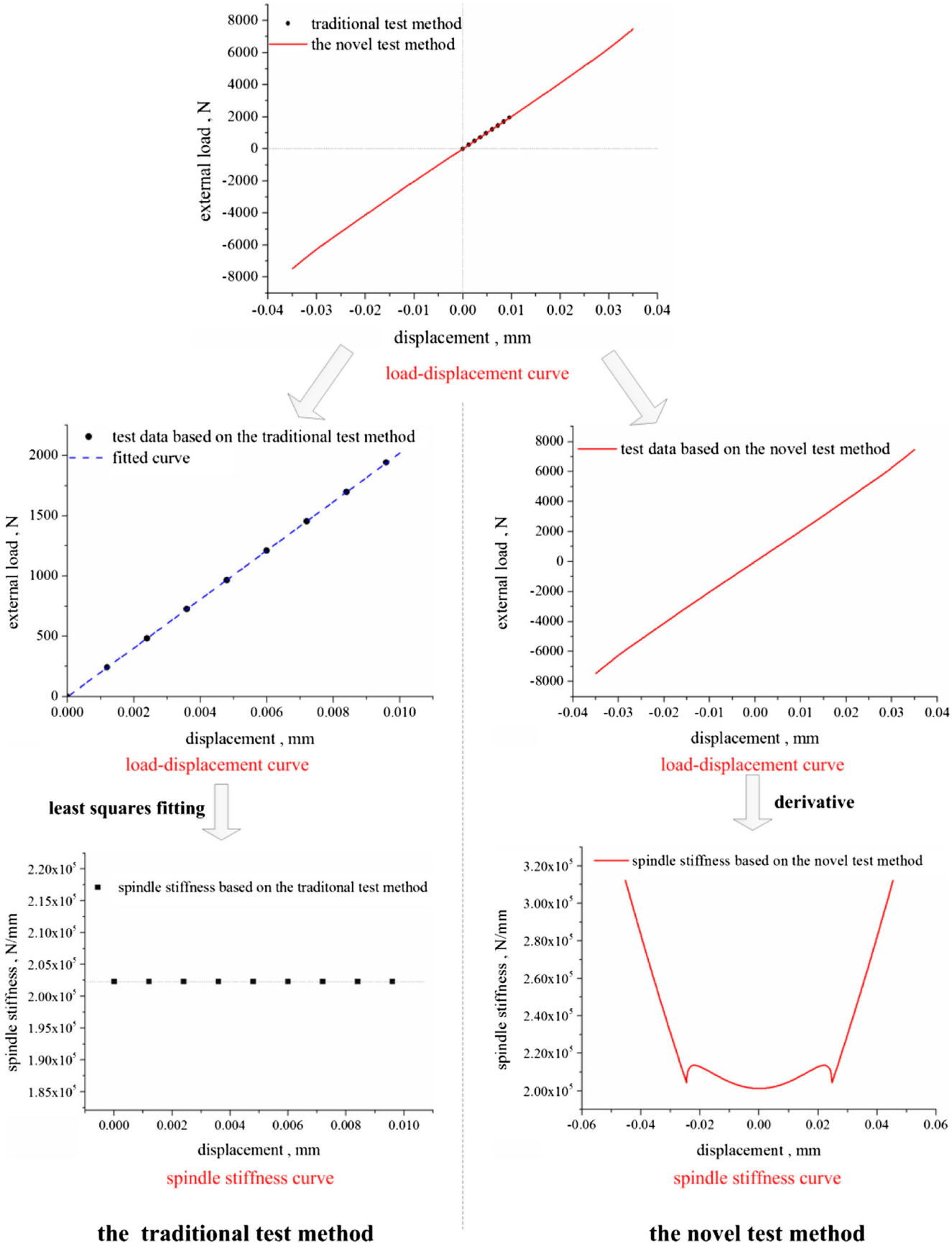

Fig. 3 Comparison of spindle stiffness test methods (schematic diagram)

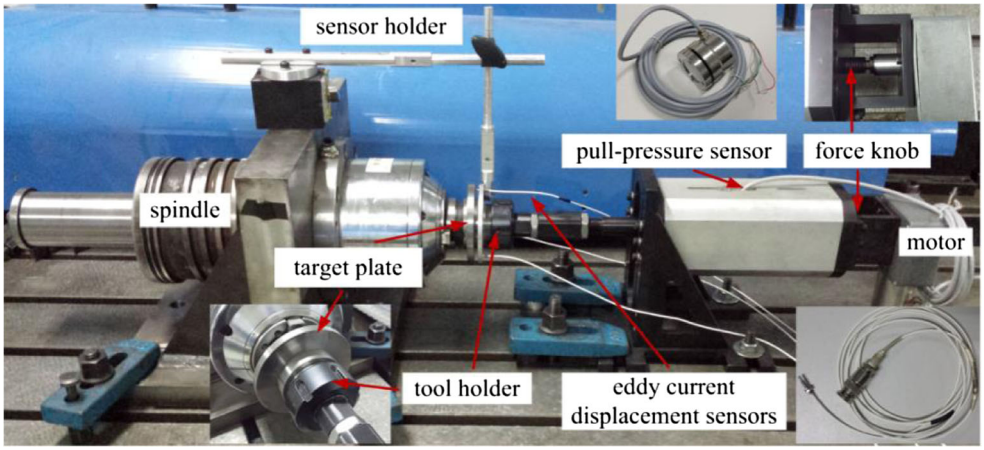

Fig. 4 Spindle stiffness test rig

for the case of preload 290 N, the stiffness presents a relatively constant value with the change of the axial load.

The spindle stiffness would exhibit the characteristics of softening or hardening as the external load changes, which is related to the applied preload. It can be inferred that there must be a suitable preload so that the spindle stiffness remains relatively constant over a certain range.

3 Theoretical analysis of experimental results

In this section, the load–displacement model of the bearing is first established to theoretically explore the above experimental phenomenon. Base on the bearing model, the axial stiffness model of the spindle is proposed. Through changing the preload parameters in the spindle model, the variation mechanism of the spindle axial stiffness under different preload is studied.

3.1 Axial load–displacement model of bearing

The bearing model established in this section is under the condition of pure axial load and no radial load. This model can be solved by the following steps (illustrated in Fig. 7). Firstly, the operating contact angle of the bearing is obtained through Eq. (2). Then, bearing normal deflection constant is calculated by Eq. (3). Finally, the bearing axial load can be obtained.

According to Ref. [29], bearing operating contact angle under pure axial load can be calculated as:

$$\alpha = \arcsin\left(\frac{A_o \sin\alpha_f + \delta_{ab}}{\sqrt{A_o^2\cos^2\alpha_f + \left(A_o\sin\alpha_f + \delta_{ab}\right)^2}}\right) \tag{2}$$

where α is the operating contact angle of the bearing; A_o means the distance between raceway groove curvature

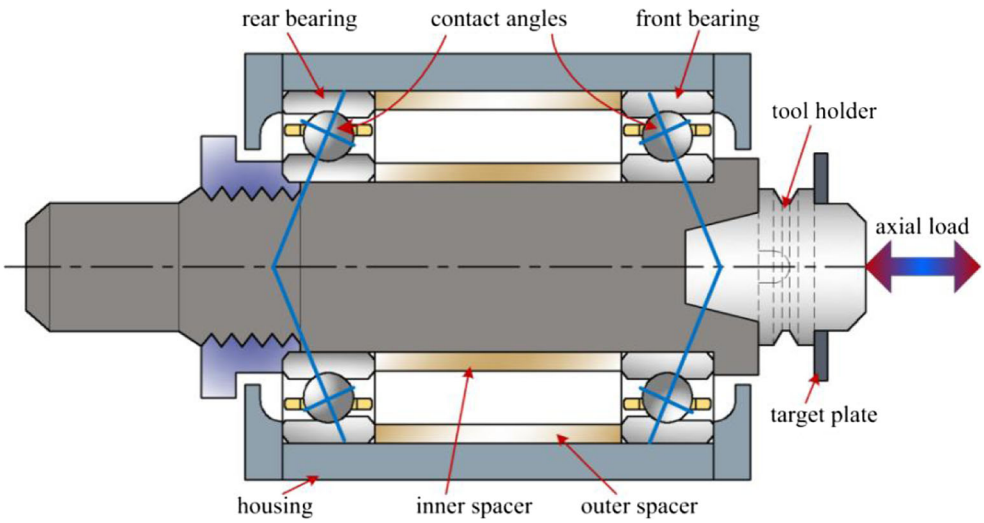

Fig. 5 Structure of experimental spindle

Table 2 Preload level of bearing 7014CTYNSULP4 [18]

Preload level	EL	L	M
Spindle preload (N)	145	290	740

centers; α_f indicates the initial contact angle of the bearing; δ_{ab} is the axial displacement of the bearing.

K_f, bearing normal deflection constant, can be derived from the load-deflection coefficient of bearing inner ring and outer ring k_i, k_o:

$$K_f = \left[\left(\frac{1}{k_o}\right)^{2/3} + \left(\frac{1}{k_i}\right)^{2/3}\right]^{-\frac{3}{2}} \tag{3}$$

where load-deflection coefficient of inner ring and outer ring k_i, k_o can be obtained by Eqs. (4) and (5), ρ_1 and ρ_2 are principal curvatures, the subscripts i and o respectively denote bearing inner ring and outer ring, which can be calculated by Eqs. (6) and (8) and Eqs. (7) and (9). d_b means the ball diameter, d_m is the bearing pitch diameter, and R equals the groove curvature radius. E_i^* and E_o^* are the equivalent Young's modulus and can be calculated by Eq. (10) and Eq. (11). ν denotes the Poisson's ratio of the material, E denotes Young's modulus of material, and subscripts ir, or, and b are the material of inner ring, outer ring, and balls, respectively.

$$k_i = 0.5973\left(\frac{\rho_{2i}}{\rho_{1i}}\right)^{0.345}\rho_{2i}^{-0.5}E_i^* \tag{4}$$

$$k_o = 0.5973\left(\frac{\rho_{2o}}{\rho_{1o}}\right)^{0.345}\rho_{2o}^{-0.5}E_o^* \tag{5}$$

$$\rho_{1i} = \frac{2}{d_b} - \frac{1}{R_i} \tag{6}$$

$$\rho_{2i} = \frac{2}{d_b} + \frac{2\cos\alpha}{d_m - d_b\cos\alpha} \tag{7}$$

$$\rho_{1o} = \frac{2}{d_b} - \frac{1}{R_o} \tag{8}$$

$$\rho_{2o} = \frac{2}{d_b} - \frac{2\cos\alpha}{d_m + d_b\cos\alpha} \tag{9}$$

$$\frac{1}{E_i^*} = \frac{1}{2}\left(\frac{1-\nu_b^2}{E_b} + \frac{1-\nu_{ir}^2}{E_{ir}}\right) \tag{10}$$

$$\frac{1}{E_o^*} = \frac{1}{2}\left(\frac{1-\nu_b^2}{E_b} + \frac{1-\nu_{or}^2}{E_{or}}\right) \tag{11}$$

Finally, bearing axial load F_{ab} can be obtained by Eq. (12) [30, 31]:

$$\frac{F_{ab}}{ZK_fA_o^{\frac{3}{2}}} = \sin\alpha\left(\frac{\cos\alpha_f}{\cos\alpha} - 1\right)^{1.5} \tag{12}$$

where Z refers to the number of balls.

3.2 Axial load–displacement model of fixed position preload spindle

Fixed position preload means that the axial position of spindle bearings keeps constant during spindle operation, as shown in Fig. 5.

The relation between the axial load F_{ab} and the axial displacement δ_{ab} of the angular contact ball bearing, under pure axial load, can be obtained according to Section 3.1. Here, F_{ab} and δ_{ab} satisfy the following relationship for convenience:

$$F_{ab} = f(\delta_{ab}) \tag{13}$$

where $f(\cdot)$ means the nonlinear mapping function.

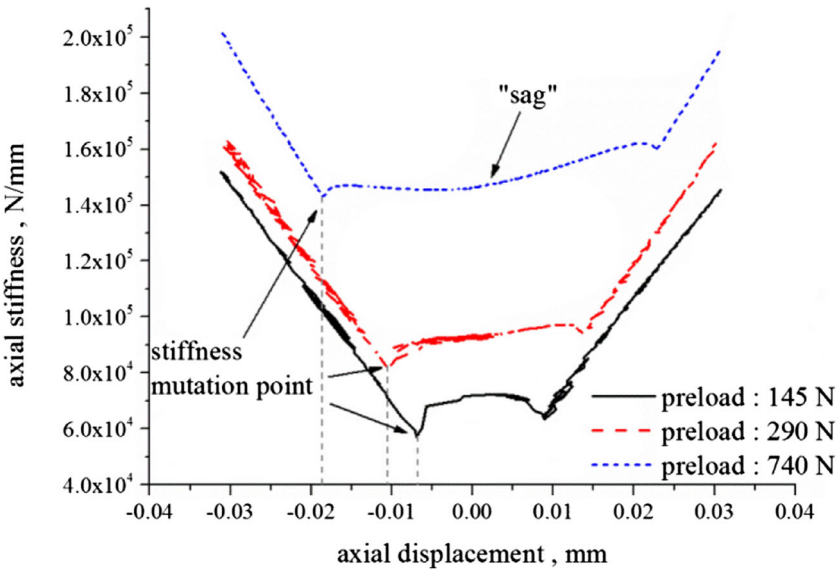

Fig. 6 The experimental results of spindle axial stiffness

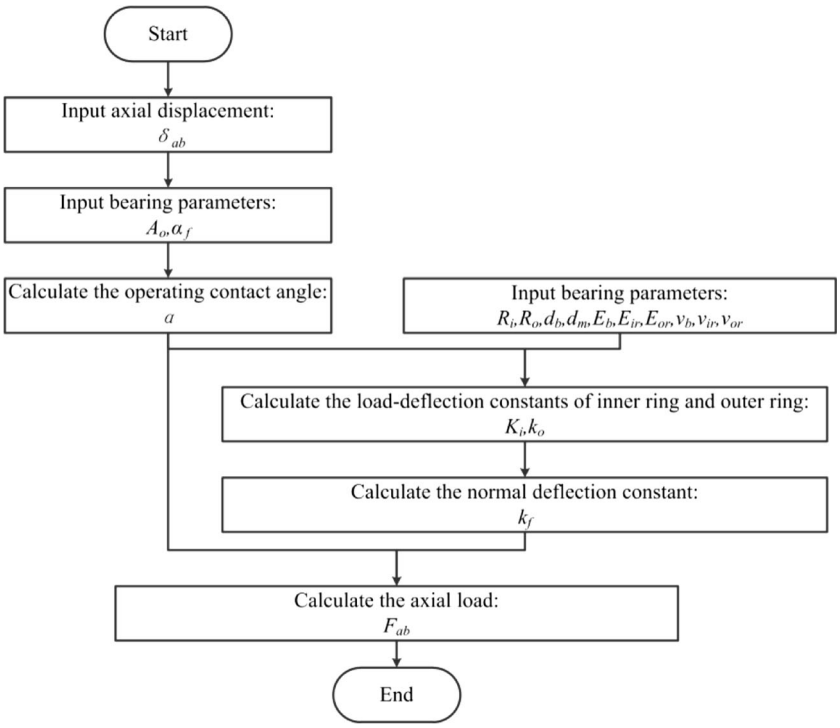

Fig. 7 Calculation flow chart

For two back-to-back mounted bearings with preload F_p, the relation between bearing load and the external axial load F_a applied to the spindle is shown in Fig. 8.

As shown in Fig. 8a, the intersection of the bearing load–displacement curves determines the amount of preload F_p and pre-deflections δ_1, δ_2, which satisfies the following relationship:

$$F_p = f(\delta_1) = f(\delta_2) \tag{14}$$

where δ_1 donates the pre-deflection of front bearing; δ_2 means pre-deflection of rear bearing.

When the axial thrust load F_a is applied to the spindle (defined as a positive value), the spindle moves δ_a toward rear bearing direction, and the axial deflections of the front and rear bearings are changed to:

$$\begin{cases} \delta_1{}' = \delta_1 + \delta_a \\ \delta_2{}' = \delta_2 - \delta_a \end{cases} \tag{15}$$

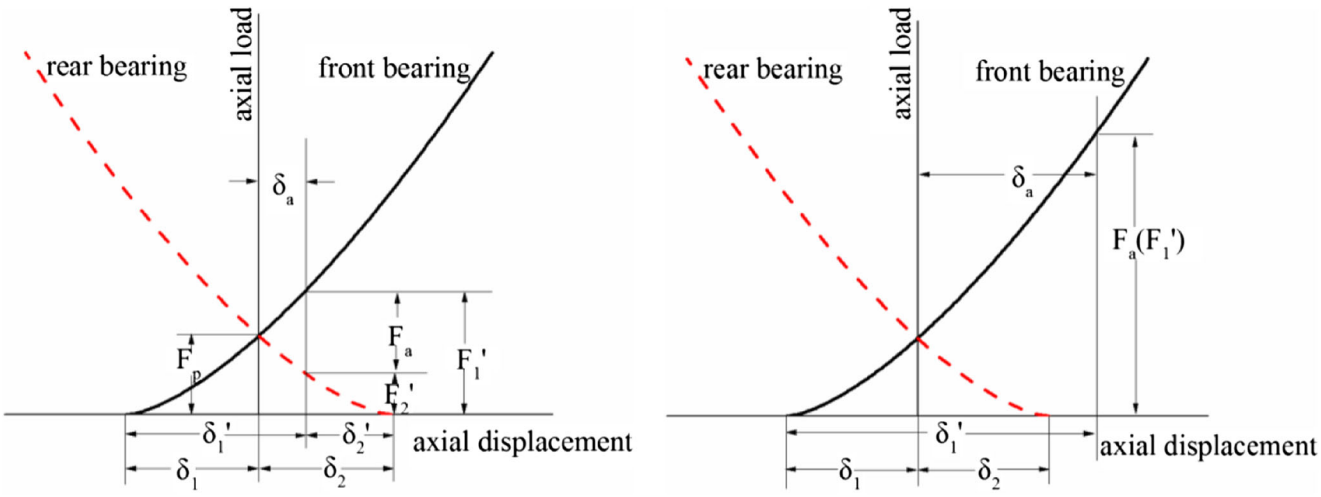

(a) One side of spindle is not completely unloaded

(b) One side of spindle is completely unloaded

Fig. 8 Load distribution of fixed position preload spindle

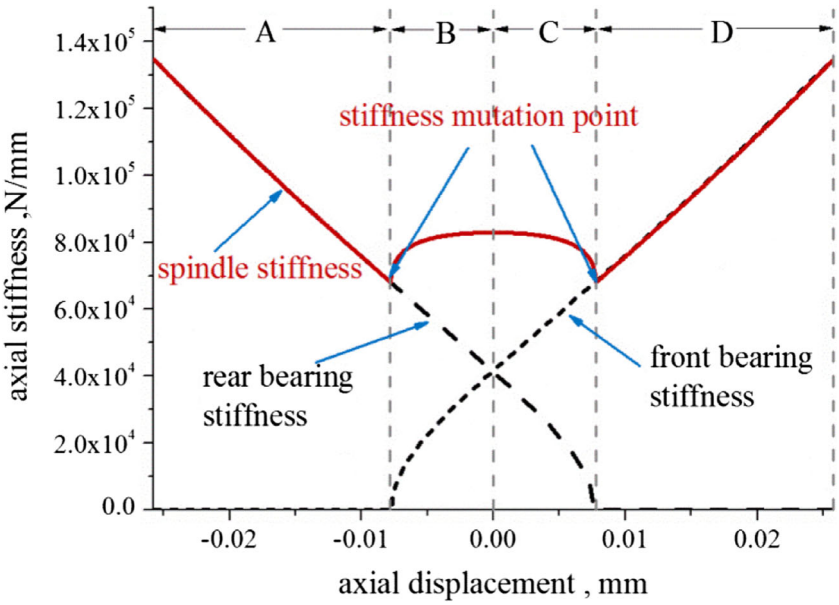

Fig. 9 The stiffness curve of fixed position preload spindle (the preload is 200 N)

Accordingly, the load applied to the front bearing increases, while the load applied to the rear bearing reduces gradually. The force balance equation of the spindle is given as:

$$f(\delta_1 + \delta_a) = F_a + f(\delta_2 - \delta_a) \tag{16}$$

As shown in Fig. 8b, as the axial thrust load increases, once the axial deflection δ_a of the spindle is greater than pre-deflection δ_2 of the rear bearing, the rear bearing is completely unloaded. Thus, the axial thrust load is completely borne by the front bearing, and the force balance equation of the spindle is as follows in this situation:

$$f(\delta_1 + \delta_a) = F_a \tag{17}$$

The analysis process is the same when the spindle is subjected to axial tension (defined as a negative value). Before the front bearing is fully unloaded, the force balance equation of the spindle is given as:

$$F_a + f(\delta_1 - \delta_a) = f(\delta_2 + \delta_a) \tag{18}$$

After the front bearing is completely unloaded, the relation can be written as:

$$F_a = f(\delta_2 + \delta_a) \tag{19}$$

Table 3 The bearing parameters

Parameters	Values	Parameters	Values
Z	20	R_i	6.19112 mm
d_b	11.906 mm	R_o	6.19112 mm
d_m	90 mm	α_f	15°

Eqs. (14)–(19) are the load–displacement models for the fixed position preload spindle and the load–displacement curve of the spindle can be obtained by solving the model.

3.3 Axial stiffness of fixed position preload spindle

The axial stiffness of the spindle can be calculated with Eq. (1) after obtaining the load–displacement data. The axial stiffness curve of the spindle was calculated, seen in Fig. 9. Spindle bearing types are all NSK® 7014CTYNSULP4. The bearing parameters are shown in Table 3.

As shown in Fig. 9, the whole loading process can be divided into four stages. In stages *A* and *B*, the spindle is subjected to axial tension, while in stages *C* and *D*, the spindle is subjected to axial thrust load. It can be seen from the spindle stiffness curve that there is stiffness mutation point at the curve junction of stages *A*(*C*) and *B*(*D*). It can be also understood that the spindle stiffness is equal to the single-end bearing stiffness in stages A and D since only single bearing bears the load in these stages.

In order to analyze the evolution of spindle stiffness, the relation between the bearing axial stiffness and the bearing axial displacement was studied. As shown in Fig. 10, the stiffness ratio, which is the first derivative of stiffness versus displacement, means the change rate of bearing axial stiffness. It can be seen that the stiffness ratio of the bearing is positive. As the axial displacement increases, the stiffness ratio of bearing decreases at first, and then it increases gradually. The results show that bearing axial stiffness is proportional to axial displacement. With the axial displacement gradually increasing, the axial stiffness of bearing increases slower and slower, then it gets faster and faster again.

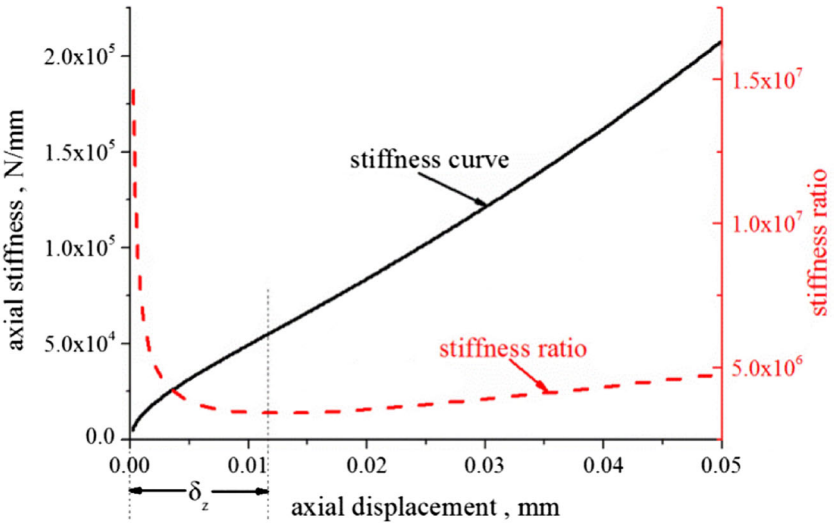

Fig. 10 Relation between axial stiffness and axial displacement of the single-end bearing

For the purpose of facilitating analysis of the spindle stiffness, the front and rear bearings are described as nonlinear springs in the stiffness analysis diagram (as shown in Fig. 11). According to the mechanical analysis of the spindle, the axial stiffness of the fixed position preload spindle exhibits the parallel relationship between the front and rear bearings stiffness (Fig. 9), namely:

$$k_a = k_{a1} + k_{a2} \tag{20}$$

where $k_a$is the axial stiffness of the spindle; k_{a1} denotes the axial stiffness of the front bearing; k_{a2} means the axial stiffness of the rear bearing.

In stage *C* (stage *B*), the spindle is initially subjected to axial load. At this stage, the axial load applied to the spindle is shared by the front and rear bearings, so the axial stiffness is determined by both of the bearings.

However, in the stage *D* (stage *A*), the axial displacement of the spindle caused by the axial load is greater than the predeflection of bearings, resulting in the complete unloading of one side bearing. In the meantime, the axial load of the spindle is borne by the other side bearing. Therefore, the spindle stiffness is converted to the single-end bearing stiffness. According to the relation between bearing axial stiffness and axial displacement (shown in Fig. 10), the spindle axial stiffness increases with the axial load at this stage.

The junction of stage *C* (stage *B*) and stage *D* (stage *A*) means that load shared by both sides of bearing changes to be borne by one side.

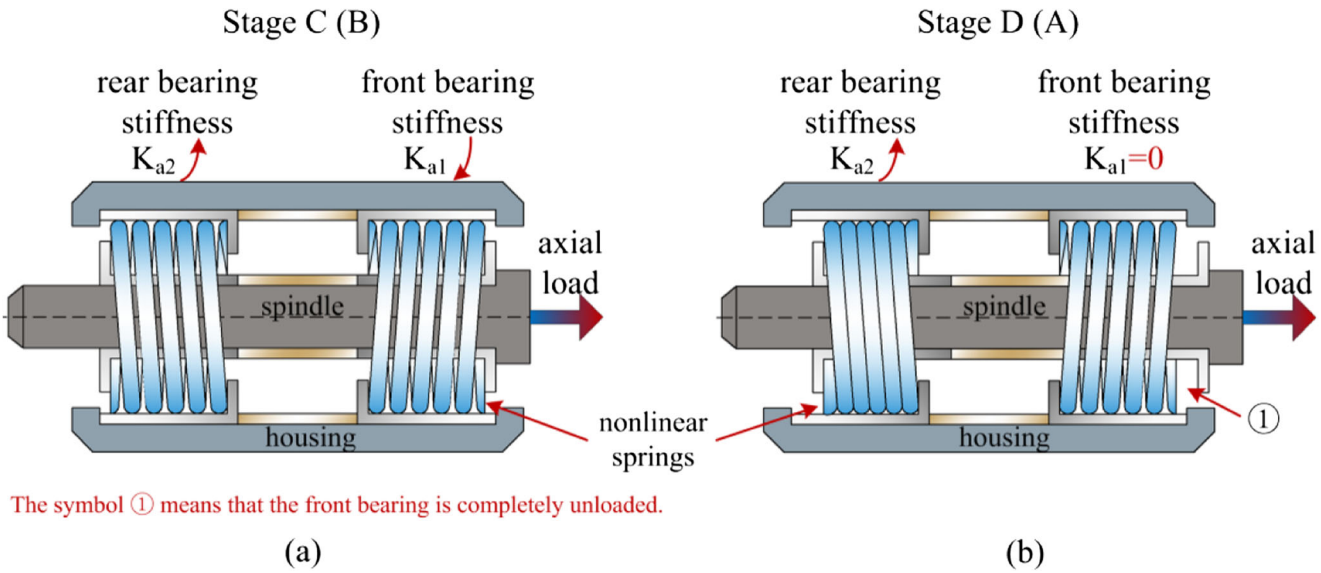

Fig. 11 Analysis diagram of fixed position preload spindle stiffness (axial tension)

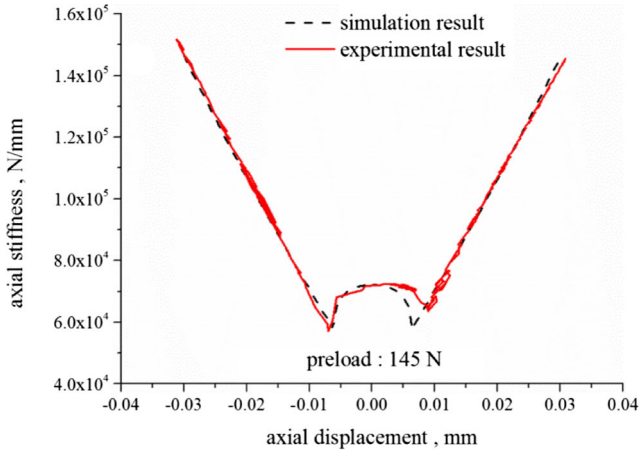

(a) bearing preload is 145N

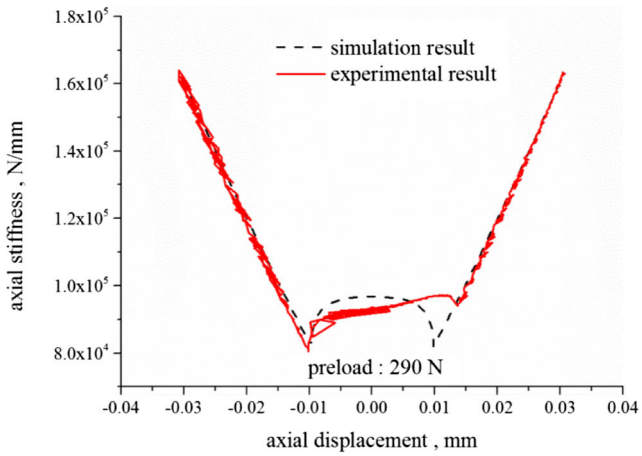

(b) bearing preload is 290N

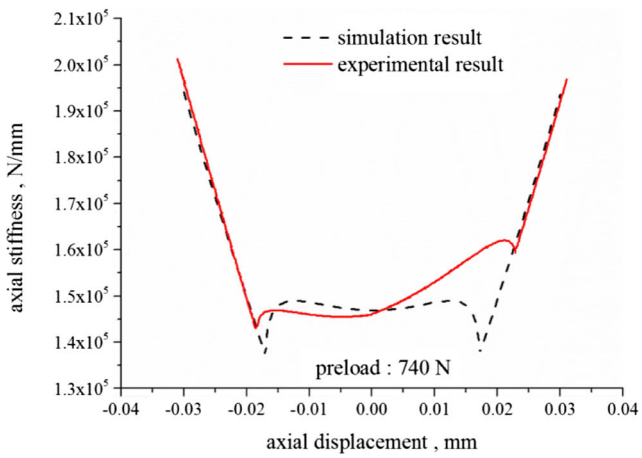

(c) bearing preload is 740N

Fig. 12 Comparison of experimental result with simulation result (the preload is 330 N), **a** bearing preload is 145 N, **b** bearing preload is 290 N, **c** bearing preload is 740 N

3.4 Model validation

The comparison of experimental result with simulation result is shown in Fig. 12.The stiffness trend of the experimental result is in agreement with that of the simulation result, the maximum errors between the simulation result and the experimental result are 18.5%, 17.4%, and 13.9%, respectively (bearing preloads are 145 N, 290 N, and 740 N). There are two main reasons for the errors. Firstly, the experimental data after filtering is distorted, and the filtering algorithm can be further improved to reduce the errors. Secondly, although the spindle stiffness is mainly determined by the bearing stiffness, the experimental spindle stiffness includes the stiffness of other spindle components, such as the draw bar mechanism. The errors can be reduced by further improving the theoretical model.

3.5 Effect of preload on spindle stiffness

As the operating conditions change, the spindle preload will be changed accordingly. According to the axial stiffness model, the stiffness curves under different preload can be calculated by changing preload F_p in Eq. (14).

It can be seen from Fig. 13 that the overall rigidity of the fixed position preload spindle increases as the preload increases. The reason is as follows. As the bearing preload increases, the pre-deflections of the front and rear bearings increase, and the bearing stiffness will increase accordingly (seen in Fig. 10). As shown in Eq. (20), the spindle stiffness is the superposition of the front and rear bearing stiffness, therefore the spindle overall stiffness would increase due to the increase in preload.

In addition, from Fig. 13 one can observe that, once the spindle stiffness changes abruptly (which means one of the bearings is completely unloaded), large axial displacement occurs in condition of large spindle preload. In other words, the greater the preload is, the larger the axial load is needed to unload single-end bearing. This is because, only when the bearing pre-deflection is completely offset by the axial load applied to the spindle, single-end bearings of the spindle will be completely unloaded, and then the spindle stiffness changes abruptly. Due to the difference in spindle preload, the pre-deflection of the bearing is not consistent. The greater the spindle preload is, the larger the pre-deflection of the bearing becomes. Only when the displacement of the spindle and the pre-deflection are equal in value, the single-end bearings of the spindle can be completely unloaded. That is to say, the spindle displacement corresponding to the mutation point of the spindle stiffness in Fig. 13 is equal to the pre-deflection of the spindle bearing.

At the same time, it is observed from Fig. 13 that there is an obvious “sag” shape in the spindle stiffness curve with large

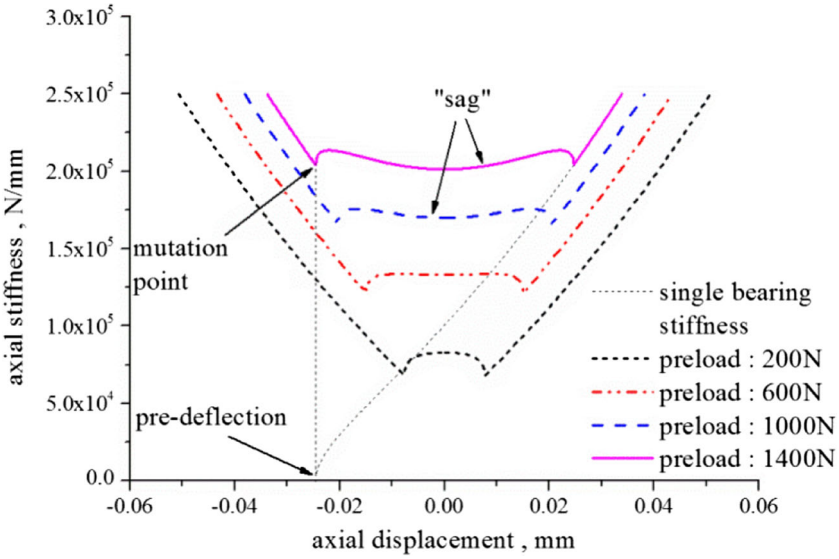

Fig. 13 The relation between the stiffness and displacement of spindle under different preload

preload. Moreover, the greater the preload is, the more obvious the "sag" shape is.

The "sag" shape of the spindle stiffness curve is dependent on the spindle preload. The single-bearing axial stiffness curve is shown in Fig. 10. The growth rate of single bearing axial stiffness presents two phases, and it is related to the initial deflection of the bearing δ_p, which decreases at first ($\delta_p < \delta_z$) and then increases ($\delta_p > \delta_z$). Thereinto, the δ_z represents the displacement corresponding to the minimum value of stiffness ratio.

In the case of $\delta_p > \delta_z$, the growth rate of the bearing stiffness increases as the displacement increases. Initially, with the axial thrust load increasing, the increment of front bearing stiffness is greater than the reduction of rear bearing stiffness. So the stiffness of spindle is increasing gradually. Since the axial pre-deflection of spindle is much greater under a larger initial preload, the "sag" shape becomes more obvious at the larger preload as shown in Fig. 13. And then, with axial load continuing to increase, the rear bearing continues to be unloaded. When $\delta_2 < \delta_z$, the decreasing rate of rear bearing stiffness becomes larger, and the increasing rate of spindle stiffness gradually slows. Once the decreasing rate of rear bearing stiffness is greater than the increasing rate of the front bearing stiffness, the spindle axial stiffness decreases with axial displacement increasing. As the axial load continues to increase, the rear bearing is completely unloaded, and the axial load is completely borne by the front bearing. At this time, the stiffness of the spindle changes into the stiffness of the front bearing. As the axial load increases, the stiffness of the spindle increases gradually.

In the case of $\delta_p \leq \delta_z$, when bearing displacement changes, the bearing stiffness decrement is greater than its increment. So the axial stiffness of spindle decreases as the axial load increases. When the axial thrust load is large enough to completely unload the rear bearing, the axial load is completely borne by the front bearing, and then the axial stiffness of the spindle increases gradually as the axial load increases. In this case, the "sag" shape disappeared in the stiffness curve.

Finally, it can be seen from Fig. 10 that bearing stiffness ratio is relatively constant near the axial displacement δ_z. At this point, the bearing stiffness increase rate is about equal to the stiffness reduction rate. If the spindle bearing initial pre-deflection is within this range, the spindle stiffness under certain load conditions will remain relatively constant, which can be used to guide the design of the machine tool spindle.

4 Conclusion

In this paper, the axial stiffness of fixed position preload spindle under different preload is experimentally measured and the evolution mechanism is analyzed. It was found in this paper that when bearing preload reaches a certain threshold, the "sag" shape appears in spindle stiffness curve, which refers to the "stiffness hardening" characteristics of the spindle. As the preload increases, the "sag" shape becomes more obvious. Namely, the stiffness of spindle increases with the increasing axial load within a certain load range.

For small preload, no "sag" shape occurs in spindle stiffness curve, which indicates that the spindle has the characteristics of "stiffness softening" (the spindle axial stiffness decreases as the axial load increases).

The paper reveals the evolution rule of spindle stiffness with the change of axial load under different preload, which is of great significance for understanding the spindle stiffness properties and optimizing the preload design.

Acknowledgments The research work was financially supported by the National Natural Science Foundation of China (grant no. 51675410), the National Science and Technology Major Project (grant no. 2012ZX04005011).

References

1. Matsubara A, Yamazaki T, Ikenaga S (2013) Non-contact measurement of spindle stiffness by using magnetic loading device. Int J Mach Tools Manuf 71(8):20–25
2. Matsubara A, Tsujimoto S, Kono D (2015) Evaluation of dynamic stiffness of machine tool spindle by non-contact excitation tests. CIRP Ann 64(1):365–368
3. Abele E, Altintas Y, Brecher C (2010) Machine tool spindle units. CIRP Ann Manuf Technol 59(2):781–802
4. Ma C, Mei X, Yang J, Zhao L, Shi H (2015) Thermal characteristics analysis and experimental study on the high-speed spindle system. Int J Adv Manuf Technol 79(1–4):469–489
5. Chen JS, Chen KW (2005) Bearing load analysis and control of a motorized high speed spindle. Int J Mach Tools Manuf 45(12–13): 1487–1493
6. Lin CW, Tu JF, Kamman J (2003) An integrated thermo-mechanical-dynamic model to characterize motorized machine tool spindles during very high speed rotation. Int J Mach Tools Manuf 43(10):1035–1050
7. Yan K, Yan B, Wang YT, Hong J, Zhang JH (2018) Study on thermal induced preload of ball bearing with temperature compensation based on state observer approach. Int J Adv Manuf Technol 94(9–12):3029–3040
8. Chen JS, Hwang YW (2006) Centrifugal force induced dynamics of a motorized high-speed spindle. Int J Adv Manuf Technol 30(1–2):10–19
9. Tlusty JR, Livingston IV, Teng YB (1986) Nonlinearities in spindle bearings and their effects. CIRP Ann Manuf Technol 35(1):269–273
10. Soon MP, Stone BJ (1998) The stiffness of statically indeterminate spindle systems with nonlinear bearings. Int J Adv Manuf Technol 14(11):787–794
11. Rabréau C, Noël D, Loch SL, Ritou M, Furet B (2017) Phenomenological model of preloaded spindle behavior at high speed. Int J Adv Manuf Technol 90(9–12):1–12
12. Zivkovic A, Zeljkovic M, Tabakovic S, Milojevic Z (2015) Mathematical modeling and experimental testing of high-speed spindle behavior. Int J Adv Manuf Technol 77(5–8):1071–1086
13. Sarhan AAD, Matsubara A, Sugihara M, Saraie H, Ibaraki S, Kakino Y (2006) Monitoring method of cutting force by using additional spindle sensors. JSME Int J Ser C Mech Syst Mach Elem Manuf 49(2):307–315
14. Sarhan AAD, Matsubara A (2015) Investigation about the characterization of machine tool spindle stiffness for intelligent CNC end milling. Robot Comput Integr Manuf 34:133–139
15. Tsuneyoshi T (2007) Spindle preload measurement and analysis. Proc. of the 2007 ASPE summer topical meeting, ASPE, June 11 and 12, State College, PA, pp. 35–38
16. Li JD, Zhu YS, Xiong QQ, Yan K (2014) Research on axial dynamic stiffness of fixed-pressure spindle. J Xi'an Jiaotong Univ 48(10):126–130
17. Cao H, Holkup T, Altintas Y (2011) A comparative study on the dynamics of high speed spindles with respect to different preload mechanisms. Int J Adv Manuf Technol 57(9–12):871–883
18. NSK (2006) Catalogue-super precision bearing. http://www.nsk.com/common/data/ctrgPdf/e1254h.pdf
19. Yamazaki T, Matsubara A, Fujita T, Muraki T, Asano K, Kawashima K (2010) Measurement of spindle rigidity by using a magnet loader. J Adv Mech Des Syst Manuf 4(5):985–994
20. Feng M, Yang W, Li C (2013) Advances in performance testing technology for high-speed spindles (electric spindles) of machine tools. Manuf Technol Equip Market 3:69–73
21. Feng M, Zhao YL, Yang W, Deng YZ (2013) The development of non-contact gas-loading system for stiffness measurement of high-speed spindles. Mach Des Manuf 6:102–105
22. Lu C (2011) Research on displacement detection technology of axial magnetic suspension bearing. Doctoral dissertation, Nanjing University of Science and Technology
23. Cao PH (2017) Research on radial measurement method of rotor axial displacement. Master Dissertation, Xi'an Jiaotong University
24. Yang G (2008) High speed electronic spindle turning precision and static stiffness testing research. Doctoral dissertation, Chongqing University
25. Harris TA, Kotzalas MN (2006) Advanced concepts of bearing technology. Taylor & Francis, Boca Raton
26. Zhang JH, Fang B, Hong J, Zhu YS (2017) Effect of preload on ball–raceway contact state and fatigue life of angular contact ball bearing. Tribol Int 114:365–372
27. Zhang JH, Fang B, Zhu YS, Hong J (2017) A comparative study and stiffness analysis of angular contact ball bearings under different preload mechanisms. Mech Mach Theory 115:1–17
28. Halicioglu R, Dulger LC, Bozdana AT (2016) Structural design and analysis of a servo crank press. Eng Sci Technol Int J 19(4):2060–2072
29. Guo XN (2002) Analysis and calculation of angular contact ball bearings contact angle under pure axial load. Wazhou Sci Technol 1:22–24
30. Antoine JF, Abba G, Molinari A (2006) A new proposal for explicit angle calculation in angular contact ball bearing. J Mech Des 128(2):468–478
31. Harris TA, Kotzalas MN (2006) Essential concepts of bearing technology. Taylor & Francis, Boca Raton